16B.7 ELECTRIFICATION AND LIGHTNING IN AN IDEALIZED BOUNDARY-CROSSING SUPERCELL SIMULATION OF 2 JUNE 1995

Alexandre O. Fierro[*3,4], Matthew S. Gilmore[1,2,3], Louis J. Wicker[3], Edward R. Mansell[1,3], Jerry M. Straka[4], Erik N. Rasmussen[1,3]
[1] Cooperative Institute for Mesoscale Meteorological Studies, Univ. of Oklahoma, Norman, Oklahoma
[2]Dept. of Atmospheric Sciences, Univ. of Illinois, Urbana, Illinois
[3]NOAA/ NSSL, Norman, Oklahoma
[4]School of Meteorology, Univ. of Oklahoma, Norman, Oklahoma

1. INTRODUCTION*

On 2 June 1995, 11 thunderstorms intensified after crossing a preexisting outflow boundary in West Texas and many increased in positive cloud-to-ground (+CG) flash rates (Gilmore and Wicker, 2002, hereafter GW02). Of interest is to understand how changes in the supercell kinematics and microphysics associated with intensification influence storm charge separation, charge structure, CG lightning flash rate, and dominant CG polarity in simulated storms based upon the 2 June 1995 case. The work herein improves upon previous idealized boundary-crossing simulations from Gilmore and Wicker (1998b) and Gilmore et al. (2002) in that the numerical cloud model incorporates more sophisticated microphysics (Straka and Mansell 2004) and a lightning model (Mansell et al. 2002)

2. EXPERIMENTAL DESIGN

All simulations were carried out for four hours in a 191 km x 125 km x 22 km domain with a resolution of $\Delta x=\Delta y=\Delta z$ = 600 m for the lightning grid and half the horizontal resolution for the microphysics and kinematic variables. A stretched vertical grid was also used to better resolve the flow in the boundary layer (Δz = 100 m near the surface stretched to 600 m at and above 7 km AGL).

2.1. Initial conditions

Two (one) soundings were (was) used for the initialization of the heterogeneous (homogeneous) environment. Of the two, the "cool side" sounding has the greatest low-level shear, CAPE, and boundary layer moisture (Fig. 1; see discussion in GW02). The “warm side" sounding was used as base state for the homogeneous simulations (Fig 1a, red dashed line). The boundary (or heterogeneous domain) was initialized using an inverse hyperbolic tangent function (as in Gilmore et al. 2002) between the warm side and the cool side sounding. This smooth transition between both

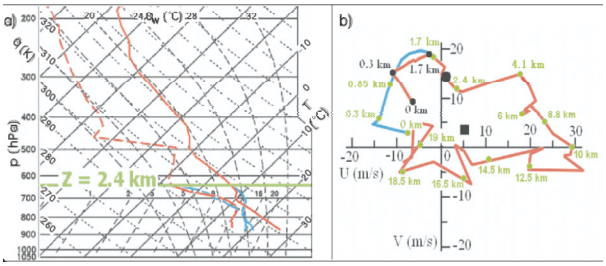

Fig. 1. (a) Skew T–log p diagrams and (b) hodographs used to define the initial conditions on the warm (red) and cool (blue) sides of the boundary. Hodograph altitudes are marked in green everywhere except below z = 2.4 km where the warm side hodograph altitudes are shown with black dots. The large circle (square) shows the ground relative velocity of the strongest right moving cell (R1) while on the warm (cool) side of the boundary.

environments was only applied below 2.4 km where most of the environmental changes were observed and to prevent solenoidal circulations aloft. Above 2.4 km, the warm side sounding was used. Moreover, both wind profiles (Fig 1b) were rotated 45 degrees clockwise to have a NW-SE boundary orientation parallel to the lateral domain's y-axis.

Following Gilmore et al. (2002) the soundings used in the model are based upon those observed near Hub, Texas (closest to storm initiation locations on the warm side) and Lockney, Texas (on the immediate cool side). Additionally, the following modification were applied:

- The warm-side sounding values of q_v were reduced via trial and error between 1 and 1.95 km (near the LCL) and above 11.5 km, to limit secondary cell development and to prevent upper-level formation of ambient cirrus cloud, respectively.
- The cool side sounding values of T between z = 1.25 and 2.35 km were increased slightly (increasing the CIN) to limit secondary cell development on the cool side of the boundary.

Storms were initiated within the "warm side" environment with a thermal bubble centered at 1.5 km AGL with a +3 K anomaly with horizontal and vertical radii of 10 km and 1.5 km, respectively. The initial bubble (boundary) location was positioned 1/3 (2/3) of

* *Corresponding author address:* Alexandre O. Fierro, School of Meteorology, Univ. of Oklahoma
E-mail: Alexander.fierro@noaa.gov.

the way across the domain such that the initial (and strongest) right-moving storm R1 crossed the boundary at about t = 2 h. The boundary moved toward the storm (SW) at an average ground-relative speed of ~4 m s^{-1}.

3. EXPERIMENTAL METHODOLOGY

3.1. General overview

Motivated from the observational hypotheses of GW02, the first goal of this work was to determine qualitatively and quantitatively how the simulated supercell's kinematics and microphysics responded to the change in environmental conditions as it crossed the boundary. The second goal was to test how this intensification influenced storm electrification, charge structure, and lightning for four different non-inductive (NI) charging schemes.

3.2. Model charging and microphysics schemes

Four NI charging schemes were tested: Gardiner et al. (1985, hereafter Gardiner) modified following Ziegler et al. (1991), Saunders et al. (1991, hereafter S91) modified following Helsdon et al. (2001), Saunders and Peck (1998, hereafter SP98) modified following Mansell et al. (2003), and Riming Rate (hereafter RR; Mansell et al. 2003). Each of the four schemes are based upon laboratory experiments where collisional charging was measured between ice crystals and a riming rod (simulated graupel) in the presence of supercooled liquid water. This process is believed to account for much of the observed electric fields in thunderstorms.

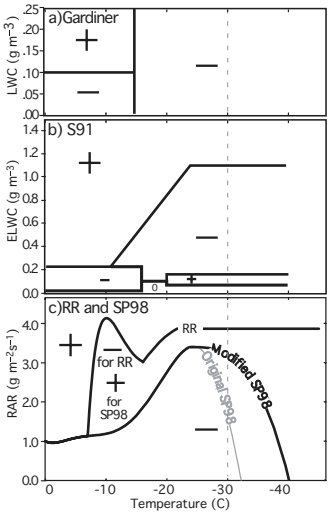

Fig. 2. Respective critical curve diagrams of (a) the Gardiner et al (1985) NI scheme adapted by Ziegler et al. (1991), (b) the Saunders et al. (1991) NI scheme as modified by Brooks et al (1997) and Helsdon et al. (2001) and (c) the Saunders and Peck (1998) and Riming Rate (Mansell et al. 2003) NI schemes. The SP98 critical curve used for this study was modified by Mansell et al. (2003) and is shown by "Modified SP98". The charging sign acquired by graupel is shown for each region. All diagrams extrapolate below T = –30 C.

The difference among these schemes is attributed to different laboratory conditions and to the choice of how cloud water is represented (Fig. 2). [The Takahashi (1978) scheme was not selected since it is incapable of producing +CG flashes in multicell and supercell storms in the current version of the model (Mansell et al. 2002, 2003).]

The coefficients controlling inductive charging were unchanged for the four cases. However, the magnitude of inductive charging is a function of the local electric field (produced initially by NI charging). Thus, inductive charging also differed throughout the domain between the four NI schemes tested.

4. RESULTS AND DISCUSSION

4.1. Kinematic and microphysics evolution in homogeneous and heterogeneous environments

Data was extracted and analyzed using a box following the strongest right-moving cell (R1) in this study (lateral edges of this box are shown in Fig. 3). Thus, all the plots shown herein will focus on R1 only.

As expected, the initial evolution (until ~80 min) of R1 kinematics and microphysics was similar in the homogeneous and heterogeneous cases (Figs. 3 and 4). Later, as R1 crossed the boundary (t = 120 min; Fig. 3b), it significantly increased in maximum updraft speed at mid and low-levels (Fig. 4a), 40 dBZ echo top height (Fig. 4b), maximum low-level rotation (Fig. 4c) and 20 m s^{-1} updraft volume (not shown), which indicated a stronger and more mature supercell. The midlevel updraft speed reached its maximum after crossing the boundary and remained sustained for about 40 min. Additionally, after crossing, R1 increased in maximum radar reflectivity (Figs. 3 and 4b), hail and graupel mixing ratio (not shown), hail and graupel volume (Fig. 4d, not shown for hail). These quantities increased further after the reflectivity cores of storms R1

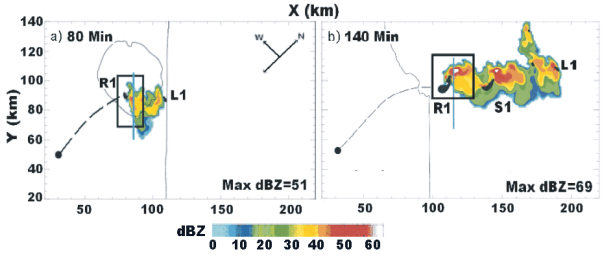

Fig. 3. Simulated radar reflectivity at z = 1.5 km in the heterogeneous environment (a) before R1 crosses the boundary (t = 80 min), (b) after R1 crosses the boundary (t = 140 min). The black-filled contours represent updraft speeds greater than 15 m s^{-1} (at z = 5 km). The thin black lines are the surface potential temperature perturbation of –1 K relative to the warm side of the boundary. The dotted line represents the track of storm R1. The secondary supercell storm that forms on the boundary at t = 90 min is labeled S1 and the left-moving supercell storm is labeled L1. The thick NW-SE line bisecting the storm depicts the location of the vertical cross sections shown in Fig. 5.

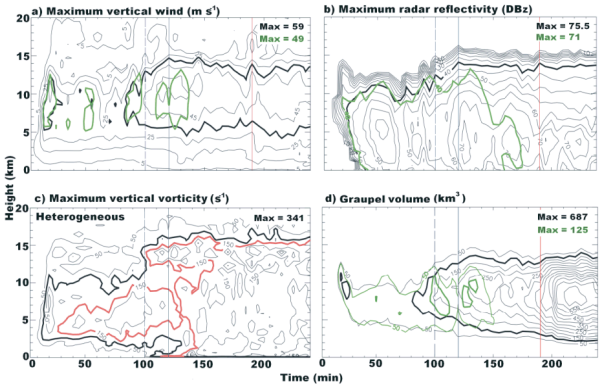

Fig. 4. Time-height contour plot of (a) maximum vertical updraft speed (m s^{-1}), (b) maximum radar reflectivity (c) maximum cyclonic vertical vorticity ($\times 10^4$ s^{-1}) for the heterogeneous case, and (d) graupel volume for the heterogeneous environment (black) and homogeneous environment (green) cases. Several thin contour lines are shown for the heterogeneous case at regular intervals (marked) with one contour thickened for comparison with a contour from the homogeneous simulation. The comparison contours in (a), (b), (c) and (d), are 35 m s^{-1}, 40 dBZ, 150 s^{-1}, and 10 & 20 km^3 respectively. In (c), only selected outer-most contours are shown and the homogeneous case is omitted.

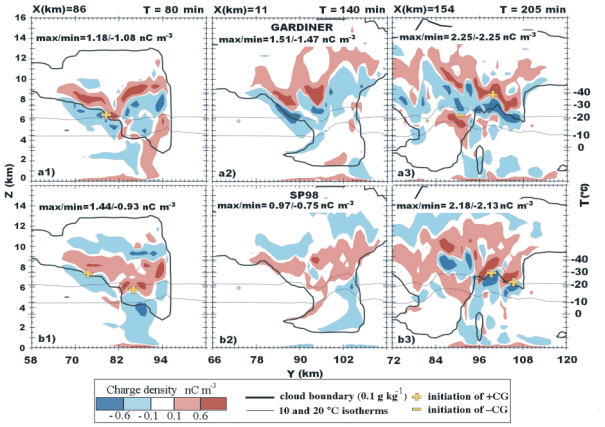

Fig. 5. Vertical cross sections in the NW-SE direction of net charge density (nC m^{-3}) and CG initiation locations for the heterogeneous environment and NI charging schemes of a) Gardiner and b) SP98. Cross sections are shown at three separate times: (a1-b1) t=80 min, (a2-b2) t=140 min, and (a3-b3) t=205 min, which represents the times before crossing, just after crossing, and after the reflectivity merger, respectively Red (blue) colors indicate positive (negative) charge density and yellow symbols indicate the locations of +CG and –CG initiation within ±15 min of the slice time and within a few gridpoints orthogonal to the slice.

and S1 merged ~70 min after R1 crossed the boundary.

S1 formed as the low-level outflow from L1 and R1 collided with the boundary. No merger of 15 m s^{-1} updraft volumes occurred between S1 and any other storm's at this time. However, the storm precipitation regions for R1 and S1 did slowly merge: graupel mixing ratio (not shown) and volume increased at low levels (Figs. 4d), resulting in larger areas and magnitudes of radar reflectivity there (Figs. 3 and 4b). However, it is unclear how much of these increases during this time were attributed to R1's intensification after crossing versus the gradual merger with S1. By t = 190 min, the 45 dBZ core regions of both storms at z = 1.5 km had merged – coincident with the largest relative increase in graupel and hail volume there (Fig. 4d, not shown for hail). To capture the merger, the box following R1 was increased by 44% after 205 min (Fig. 3).

In the homogeneous case, even during R1's strongest intensification phase, these kinematic and microphysics variables did not experience similar large increases (green contours in Figs. 4a-b, and 4d). Also, R1 became outflow-dominated and dissipated near 150 min (not shown), while R1 in the heterogeneous environment survived through the four hours of simulation. Hence, the new environment in the heterogeneous case was critical for intensifying and sustaining R1.

4.2. Charge structure in relation to kinematics and microphysics

Fig. 5 below shows the evolution of R1 charge structure for each of the four cases. Direct comparison is allowed by using a common cross section time and location for each case (shown in Fig. 3). When the cross section was shifted, small differences in the charge structure were observed primary within R1's downdraft region.

At t = 80 min (or in the homogeneous case at t=120 min, not shown) within the updraft region, both SP98 and RR storms exhibited an inverted tripole (two negative charge regions enclosing a midlevel positive charge region; not shown for RR), while the S91 and Gardiner cases showed a normal tripole (two positive charge regions enclosing a midlevel negative charge region). These structures are demonstrated in Fig. 5 for the Gardiner and SP98 cases.

After crossing at t = 140 min, the magnitude of the lower charge region within the updraft weakened in all four cases (e.g., two of the cases in Fig. 5). The strengthened updraft lofted the charge-carrying graupel (upward-sloping graupel contours and increased graupel volume aloft in Fig. 4d) along with the middle and upper charge regions (Fig. 5) consistent with the McGorman et al. (1989) hypothesis.

4.3. Lightning activity

The lofting of R1's midlevel and upper level charge regions caused the IC flashes to initiate higher (not shown). This relative increase aloft and reduction below might accounts for almost- constant trend of total IC rate between 90 and 150 min (Fig. 6). Nevertheless, a significant relative increase in total IC flash rate occurred after ~175 min (Fig. 6), consistent with enhanced collisional charging rate during the merger as increased graupel terminal fallspeed and number

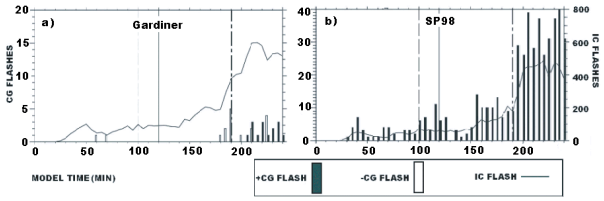

Fig. 6. Time series plots of 5-min counts of simulated positive CG, negative CG, and IC lightning flashes for the heterogeneous simulation of (a) Gardiner and (b) SP98.

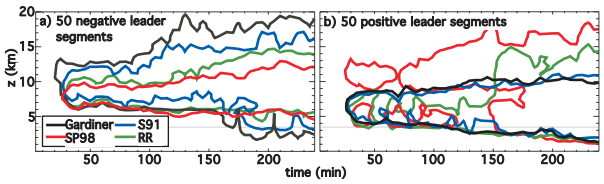

Fig. 7: As in Fig. 4 but contoured for 50 total (a) negative leader segments and (b) positive leader segments for the four NI schemes (Gardiner, S91, SP98 and RR). Inside each contour, the total amount of (horizontally integrated) leaders is greater than 50.

concentration (Fig. 4d) occurred over a larger area owing to greater areal and volume extent of graupel.

Enhanced downward graupel flux to low levels (Fig. 4d) was coincident with the descent of the leaders (Fig. 7) and with greater CG flash rate (Fig. 6). Interestingly in all four cases the positive leaders gradually descended to lower altitudes after R1 crossed the boundary, which is not true for the negative leaders (Fig. 7). This is consistent with the development/ enhancement of a negative charge at low levels (z = 0.5 – 4 km) in all cases (Figs. 5a3, 5b3) after crossing. Although only the 50 contour is shown in Fig. 7 the behavior was consistent no matter what contour from 1 to 500 was selected for display.

5. DISCUSSION AND CONCLUDING REMARKS

We have shown that the subsequent changes in the storm's kinematic and microphysical state associated with intensification after crossing the boundary had a significant impact on the evolution of the simulated storm charge structure and lightning.

Consistent with Gilmore et al. (2002), R1 increased in 40 dBZ echo top, updraft speed, and low-level mesocyclone rotation after crossing the boundary. The sustained intense updraft after crossing lofted the charged particles. R1 intensification on the cool side was also important for enhancing graupel and hail volumes, inductive charging rates (ICR), and NI charging rates (NICR), leading to deeper and stronger charge regions

The merging of the reflectivity core region between two storms was coincident with the largest relative increase of downward mass flux of graupel, allowing the development of negative charge within the downdraft and progressive positive leader descent in all four cases there. These negatively charged hail and graupel particles (via primarily NI charging) fell outside the cloud (and updraft) where liquid water content and temperatures are relatively low and thus, were able to retain much of their negative charge previously gained aloft in the main mid-to-upper main negative charge region. Moreover, inside the updraft at low levels, negative inductive charging dominated, with the exception of S91 and Gardiner where locally, pockets of positive inductive graupel charging were found which descended to low levels. In three of the four cases, this enhanced sedimentation of negatively-charged graupel after crossing (and especially after the merger) was associated with increased +CG flash rates. In contrast, none of the four homogeneous simulations (none of which included a storm merger) showed a progressive descent of the positive leaders (not shown).

We now present a conceptual model to explain the lightning behavior. First, we suggest that the midlevel charge structure that develops in each NI case pre-determines the sign of the most common downward-propagating leaders. Second, it is then the low-level charge magnitude and sign within the downdraft that determines the sign of the leaders that are able to propagate downward there. For example, for the NI schemes with a midlevel charge structure favoring downward-propagating positive (negative) leaders, the negative charge region at low levels in all four cases favors increased (reduced) positive (negative) leaders reaching ground. Further evidence of this is found in Fig. 7; the two schemes having a midlevel charge region favoring downward propagation of positive leaders (i.e. SP98 and RR) have negative leaders located at higher altitudes after ~160 min than the 2 schemes favoring downward propagation of negative leaders (Gardiner and S91). Moreover, unlike the negative leaders, the positive leaders gradually and consistently descended with time in all four cases (Fig. 7). Third, the number of leaders that reach ground (CG's) between cases is also modulated by each NI scheme's charging and leader initiation rates. That is, schemes with more downward-propagating lightning (leader) initiation aloft and/or enhanced low-level negative charge will have a greater probability for positive leaders reaching ground.

The GW02 hypothesis about greater positive NICR within the updraft is supported by the RAR-based schemes (SP98, RR), however, we have shown that one must consider the charge structure within the *downdraft* region as well to explain the CG occurrence there. Also, one cannot neglect the contribution to the charge structure from inductive charging.

At this point, the reader might wonder which of the four NI schemes tested here are correct. We do not know but suspect that none are. An argument supporting this answer is that other cells (other than the R1) forming and evolving differently (for instance S1 and L1, see Fig. 3) exhibited similar updraft charge structure and dominant CG polarity as R1 (not shown). This is

surprising given the wide variety of CG behaviors that were observed on 2 June 1995 between storms that formed in different locations with respect to the boundary (GW02). This result suggests that, provided the current microphysics, charging schemes, and resolution used in the model, these four NI charging schemes are likely incomplete and more laboratory work is needed to reconcile differences between schemes.

Finally, we emphasize that our results cannot discriminate between the relative importance of the storm intensification associated with encountering the new environment versus that associated with the precipitation merger. That is, if storm R1 had crossed the boundary but remained isolated, would similar changes in electrical behavior have occurred anyway? Furthermore, if a storm merger had occurred within the homogeneous warm side environment, would that have been sufficient to change the electrical characteristics? Answers to such questions could be addressed in future work.

6. ACKNOWLEDGMENTS

We thank the *Fulbright* Foundation for generously sponsoring Alexandre Fierro for two years and NSSL for the computing resources. Partial support for this research was also provided by NSF under grants ATM-0339519 and ATM-9986672 (M. Gilmore), ATM-9707815 and ATM-0000412 (L. Wicker), ATM-0119398 (E. Mansell and J. Straka), ATM-9617318 (J. Straka and E. Rasmussen), and the NOAA-OU Cooperative Agreement #NA17RJ1227.

7. REFERENCES

Brooks, I.M., C. P. R. Saunders, R. P. Mitzeva, and S. L. Peck, 1997: The effect on thunderstorm charging of the rate of rime accretion by graupel. *J. Atmos. Res.,* **43**, 277–295.

Gardiner, B., D. Lamb, R. L. Pitter, J. Hallet, and C. P. R. Saunders, 1985: Measurements of initial potential gradient and particles charges in a Montana thunderstorm, *J. Geophys. Res.*, **90**, 6079–6086.

Gilmore, M. S. and L. J. Wicker, E. R. Mansell, J. M. Straka, and E. N. Rasmussen 2002: Idealized boundary-crossing supercell simulations of 2 June 1995. *Preprints, 21st Conference on Severe Local Storms,* San Antonio, TX, Amer. Meteor. Soc., 251–254.

Gilmore, M. S. and L.J. Wicker, 2002: Influence of local environment on 2 June 1995 supercell cloud-to-ground lightning, radar characteristics, and severe weather on 2 June 1995. *Mon. Wea. Rev.*, **130**, 2349–2372.

Helsdon, J. H., Jr., W. A. Wojcik, and R. D. Farley, 2001: An examination of thunderstorm-charging mechanisms using a two-dimensional storm electrification model, *J. Geophys. Res.*, **106**, 1165–1192.

Mansell, E. R., D. R. MacGorman, C. L. Ziegler and J. M. Straka, 2002: Simulated three- dimensional branched lightning in a numerical thunderstorm model. *J. Geophys. Res.*, **107**, No. D9, 10.1029/2000JD000244.

Mansell, E. R., D. R. MacGorman, C. L. Ziegler and J. M. Straka, 2003: Recent results from thunderstorms electrification modeling. *Preprints, 12th International Conference on Atmospheric Electricity,* Versailles, France. Vol. I, pp 109–110.

Saunders, C. P. R., W. D. Keith, and R. P. Mitzeva, 1991: The effect of liquid water on thunderstorm charging. *J. Geophys. Res.*, **96**, 11 007–11 017.

Saunders, C. P. R., and L. S. Peck, 1998: Laboratory studies of the influence of the rime accretion rate on charge transfer during crystal/graupel collisions. *J. Geophys. Res.*, **103**, 13 949–13 956.

Straka, J. M. and E. R. Mansell, 2004: A bulk microphysics parameterization with multiple ice precipitation categories. In press at *J. Appl. Meteor.*

Takahashi, T., 1978: Riming electrification as a charge generation mechanism in thunderstorms. *J. Atmos. Sci.*, **356**, 1536–1548.

Ziegler, C. L., D. R. MacGorman, J. E. Dye, and P. S. Ray, 1991: A model evaluation of non-inductive graupel-ice charging in the early electrification of a mountain thunderstorm. *J. Geophys. Res.*, **96**, 12 833–12 855.